International Journal of GEOMATE, Oct. 2023, Vol. 25, Issue 110, pp.208-219
ISSN: 2186-2982 (P), 2186-2990 (O), Japan, DOI: https://doi.org/10.21660/2023.110.4017
Geotechnique, Construction Materials and Environment

MICROZONATION OF SEISMIC PARAMETERS IN GEOLOGICAL FORMATION UNITS ALONG THE OPAK RIVER USING MICROTREMOR MEASUREMENTS

*Nugroho Budi Wibowo[14], Teuku Faisal Fathani[2], Subagyo Pramumijoyo[3] and Gayatri Indah Marliyani [3]

[1]Doctoral Program in Geological Engineering, Faculty of Engineering, Gadjah Mada University, Indonesia;
[2]Dept. of Civil and Environmental Engineering, Faculty of Engineering, Gadjah Mada University, Indonesia;
[3]Dept. of Geological Engineering, Faculty of Engineering, Gadjah Mada University, Indonesia;
[4]Agency for Meteorology Climatology and Geophysics (BMKG), Sleman Geophysics Station, Indonesia

* Corresponding Author, Received: 10 July 2023, Revised: 9 Aug. 2023, Accepted: 16 Aug. 2023

ABSTRACT: The 2006 Yogyakarta earthquake, with a magnitude of Mw 6.3, caused significant damage primarily on the west side of the Opak River. The Opak River area encompasses formations that exhibit distinct responses to seismic wave propagation. Formations consisting of unconsolidated and young sedimentary materials tend to experience wave amplification during seismic events. This study aims to investigate the seismic wave characteristics within each formation unit using microtremor measurements. The seismic wave parameters analyzed include dominant frequency, amplification factor, shear wave velocity, weathered layer thickness, seismic vulnerability index, and lithology based on N-SPT data. The study utilized 190 microtremor data sets and 7 N-SPT data sets. The microtremor data was processed using the Horizontal to Vertical Spectral Ratio Nakamura method, while the shear wave velocity data was processed using the Imai and Tonouchi approach. The findings revealed higher amplification factors in areas dominated by unconsolidated sedimentary materials and young formations. Quaternary formations are dominated by unconsolidated sedimentary material composed of sand, silt, clay, and breccia. Formations with a tertiary age are composed of more complex lithologies such as breccia-tuff, dacite tuff, andesitic tuff, volcanic breccias, lavas, siltstone, sandstone, and conglomerate. These conditions make Quaternary formations have seismic parameter characteristics such as lower dominant frequency, higher amplification factor, thicker sediment layer thickness, and higher seismic vulnerability index compared to Tertiary formations. Quaternary formations correlate with damage to buildings after the Yogyakarta earthquake, with an average shear wave velocity character of 279-293.67 m/s, and are in a zone with a vulnerability index >20. Tertiary formations demonstrated higher seismic resistance compared to Quaternary formations, indicating their relative stability.

Keywords: Microzonation, Microtremor, Seismic parameter, Tertiary formation, Quaternary formation

1. INTRODUCTION

The Opak River flows in a northeast-to-southwest direction within the Yogyakarta region. The presence of the Opak River is closely linked to the Opak Fault, which served as the source of the 2006 Mw 6.3 Yogyakarta earthquake [1–3]. This earthquake caused significant damage to the Yogyakarta and Central Java regions, resulting in the destruction of 60,000 houses and 393 school buildings. The human toll included 6,736 fatalities, 45,210 injuries, and 33,345 displaced individuals across 95 evacuation locations [2, 4].

The extent of the earthquake's impact was not solely attributed to building-related factors but also to local geological conditions that influenced soil amplification. Soil amplification is known to occur in areas characterized by coastal alluvial deposits, decomposed and loose limestone deposits, and volcanic deposits that lack consolidation [5]. Figure 1. illustrates the distribution of damage caused by the 2006 Yogyakarta earthquake, emphasizing the prevalence of damage on the west side of the Opak River compared to its east side [6, 7]. The geological formations in the area include the Young Merapi Mountain Formations (Qmi), Alluvium (Qa), Sentolo (Tmps), Wonosari (Tmwl), Sambipitu (Tms), Nglanggran (Tmn), and Semilir (Tmse). The estimated fault line is represented by the dotted red line. The Qmi Formation, situated along the Opak River, experienced the most severe level of damage. Geologically, the Opak River is situated within the Young Merapi Volcano Deposit Formation (Qmi), which consists of undifferentiated tuff, ash, breccia, agglomerate, and lava flows. On the east side of the river lie the Nglanggran (Tmn), Semilir (Tmse), Wonosari (Tmwl), Alluvium (Qa), and Sambipitu (Tms) formations, while the west side is characterized by the Sentolo Formation (Tmps) [8].

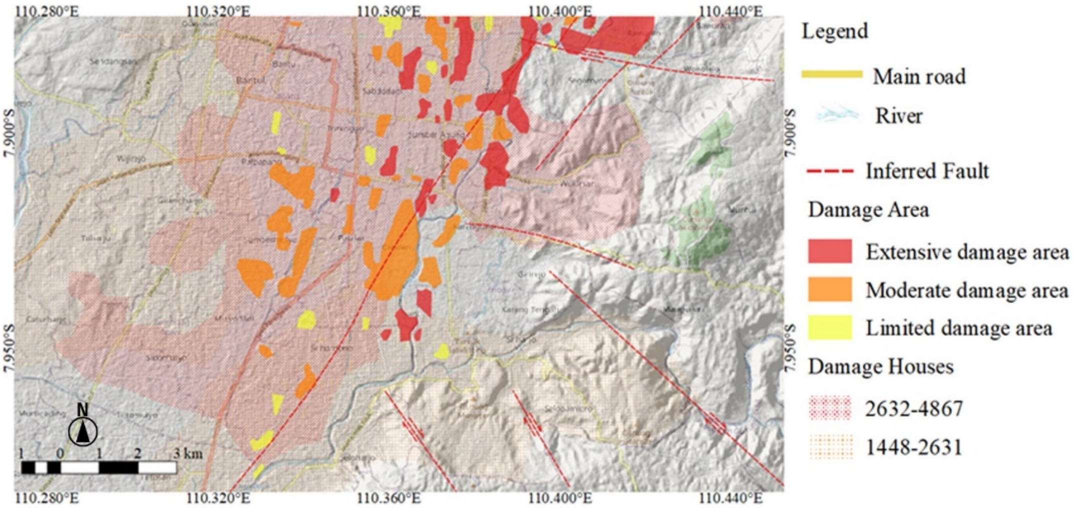

Fig.1 The map depicts the distribution of damaged buildings following the Yogyakarta Earthquake (Mw 6.3) [6–8].

The presence of these formations in the vicinity of the Opak River leads to distinct responses to surface wave propagation. Formations dominated by unconsolidated and young, weathered layers exhibit wave amplification during seismic events [9]. Conversely, formations consisting of compact and massive materials demonstrate minimal amplification or may experience wave deamplification. The phenomenon of amplification has been observed in destructive earthquakes worldwide, such as the Michoacan earthquake in Mexico (1985), Kalamata in Greece (1989), Loma Prieta in California, USA (1989), Roodbar-Manjil in Iran (1990), Kocaeli and Duzce in Turkey (1999), Chi-Chi in Taiwan (1999), Bam in Iran (2003), and Wenchuan in China (2008) [10]. This highlights the influence of lithology and rock age on seismic vulnerability in the Opak River area.

Seismic vulnerability parameters, including predominant frequency (f_o), amplification factor (A_o), weathered layer thickness (h), and seismic vulnerability index (K_g), can be determined using microtremor measurements employing the HVSR method [11–13]. These parameters vary based on the geological formations. Therefore, the objective of this study is to ascertain the seismic vulnerability characteristics within the formation units of the Opak River area and employ them in mitigation efforts.

2. RESEARCH SIGNIFICANCE

This research aims to contribute to earthquake hazard mitigation, specifically in the Opak River area, with potential applications to other regions as well. The diverse geological formations within an area exhibit varying responses to seismic wave propagation. This study will focus on characterizing the seismic vulnerability parameters within each formation, taking into account the formation's age. The seismic vulnerability parameters will be determined using microtremor measurements, N-SPT data for the v_s value approach, and lithology analysis. Within the Opak River area, the seismic vulnerability characteristics will be differentiated based on quaternary formations (Qmi and Qa) and tertiary formations (Tmps, Tmwl, Tms, Tmn, and Tmse). Understanding the seismic vulnerability of each formation will provide insights into potential damage in the event of an earthquake.

3. METHODS

This study utilized 190 data points from microtremor measurements and 7 data points from N-SPT measurements in the Opak River area (Fig.2). The microtremor data was directly collected in the field, while the N-SPT data was obtained from secondary sources at the Department of Geology, Faculty of Engineering, Gadjah Mada University. The microtremor measurements were conducted using a portable seismograph along with supporting equipment such as a geological compass, GPS, and laptop (Fig.3). The measurement duration for each microtremor point followed the operational standard of the SESAME European research project, which is 30 minutes [14]. The distribution of microtremor measurement points across each formation is as follows: Qmi Formation (85 points), Qa Formation (10 points), Tmn Formation (33 points), Tmps Formation (5 points), Tms Formation (7 points), Tmse Formation (14 points), and Tmwl Formation (36 points). The N-SPT data was collected at the locations of Segoroyoso, Karangsemut, Tempuran Opak, Bambanglipuro, Wijirejo, Pranti, and Watu.

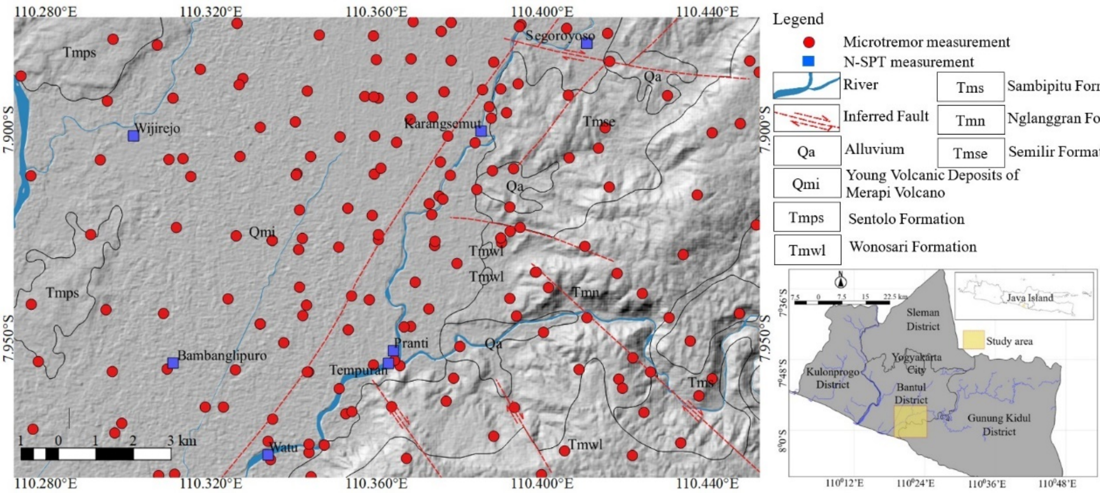

Fig.2 The red dots on the map indicate the measurement points for microtremor, while the blue boxes represent the N-SPT data points in the Opak River area. The base map used is a sheet geological map of Yogyakarta [8].

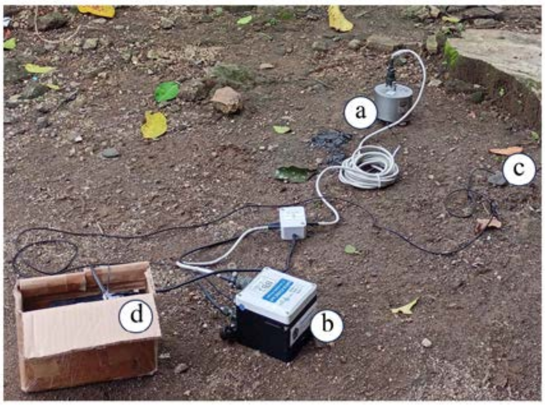

Fig.3 The process of acquiring microtremor data involves using a portable seismograph: (a) seismometer, (b) digitizer, (c) GPS and (d) battery.

Seismic vulnerability parameters derived from the microtremor data processing include predominant frequency (f_o), amplification factor (A_o), seismic vulnerability index (K_g), and weathered layer thickness parameter (h). The N-SPT data is utilized to obtain shear wave velocity (v_s) and conduct lithology analysis.

.

3.1 Microtremor and H/V Curve

A microtremor refers to a ground vibration characterized by a displacement amplitude ranging from 0.1 to 1 m and a velocity amplitude ranging from 0.001 to 0.01 cm/s [15]. The HVSR method compares the spectra of horizontal and vertical components of microtremors. The horizontal to vertical (H/V) curve is a graphical representation of the HVSR method, which is a technique for estimating the seismic characteristics of the shallow subsurface from single station acquisition. According to Nakamura [16], there exists a strong relationship between the site transfer function of shear waves and the spectrum of H/V as a function of frequency. The H/V ratio (Fig.4), which is one of the amplification factors, is closely associated with the frequency detected on the ground [16]. In 1989, the obtained data indicated that the highest value of the spectrum ratio between the horizontal and vertical components at a station located in a hard rock region was close to 1. On the other hand, the H/V maximum for a station situated in soft rocks exceeds one.

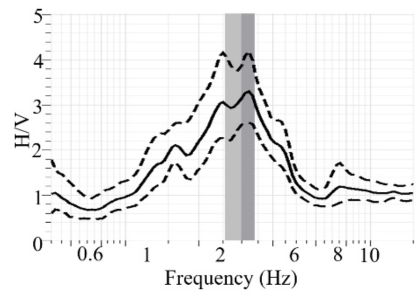

Fig.4 H/V curve, the gray box is the dominant frequency value (f_o), the dashed line is the H/V standard deviation value, the black line is the H/V value, and the peak of the black line is the H/V (A_o) value [16].

Non-natural sources of surface waves tend to propagate Rayleigh waves through soil layers or soft silt [15]. Rayleigh waves impact both the horizontal and vertical components of the surface, but they do not influence the wave component in bedrock [17]. Nakamura noted that two horizontal components are measured in the N-S and W-E directions within the observation field. This can be expressed using the following equation [16]:

$$\mathrm{HVSR} = \frac{\sqrt{(A_{(N-S)}(f))^2 + ((A_{(W-E)}(f))^2}}{(A_{(V)}(f))} \qquad (1)$$

Where:
HVSR = Horizontal to Vertical Ratio
$A_{(N-S)}(f)$ = Amplitude value of the North-South component of the frequency spectrum
$A_{(W-E)}(f)$ = Amplitude value of the West-East component of the frequency spectrum
$\left(A_{(V)}(f)\right)$ = Amplitude value of the vertical component of the frequency spectrum

3.2 Dominant Frequency (f_o) and Weathered Layer Thickness (h)

Local soil and geological conditions play a significant role in influencing the characteristics of earthquake wave propagation. Soft soils, such as weathered layers, tend to amplify ground motion at low frequencies (long periods), while hard rock tends to have minimal amplification of soil movement at high frequencies (short periods). The concept of dominant frequency is based on the closed-end organ principle [18]. The weathered layer above the bedrock is considered an open space, while the bedrock itself is viewed as a boundary or substrate. Mathematically, the dominant frequency can be formulated as shown in equation [19]:

$$v_s = \lambda \times f_o \tag{2}$$

Where λ (wavelength) equals 4 times the open space length. According to the above assumptions, the length of the open space is the thickness of the weathered layer (h). Then, the formula for the dominant frequency of the soil at depth is [19]:

$$f_o = \frac{v_s}{4h} \tag{3}$$

Where fo represents the dominant frequency of the soil measured in hertz (Hz), v_s denotes the shear wave velocity measured in meters per second (m/s), and h signifies the thickness of the weathered layer measured in meters (m). When the vibration frequency of the ground matches its natural frequency, a resonance phenomenon occurs. This resonance phenomenon leads to the amplification or magnification of waves in that particular area [19]. According to Equation (3), the value of f_o is directly proportional to the shear wave velocity and inversely proportional to the thickness of the weathered layer.

3.3 Amplification Factor (Ao)

Amplification refers to the phenomenon of seismic wave magnification caused by significant differences between layers. The amplification factor is influenced by the contrast in impedance between weathered layers and bedrock [13]. In simple terms, seismic waves experience magnification when they transition from one medium to another that is softer than the initial medium they pass through. Consequently, soft soil can lead to higher earthquake intensity compared to hard rocks at the same distance and earthquake source. The amplification value can increase when rocks undergo deformation, such as weathering, folding, or faulting, which alters their physical properties. Furthermore, within the same rock, the amplification value can vary based on the degree of deformation and weathering within the rock mass [19]. Amplification can be mathematically formulated as shown in equation [13]:

$$A_o = \frac{C_b}{C_s} \tag{4}$$

With A_o being the amplification factor, C_b being v_s in the basement layer (m/s), and C_s being v_s in the weathered layer (m/s).

3.4 Seismic Vulnerability Index (K_g)

The seismic vulnerability index (K_g) is an index that quantifies the susceptibility of the surface soil layer to deformation during an earthquake. The seismic vulnerability index is influenced by factors such as the presence of weathered layers with low solidity, while more solid and stable rocks tend to exhibit less amplification. The calculation of the seismic vulnerability index can be performed using the following equation [13]:

$$K_g = \frac{{A_o}^2}{f_o} \tag{5}$$

Where K_g represents the seismic vulnerability index, A_o denotes the amplification factor, and f_o signifies the dominant frequency measured in hertz (Hz). The seismic vulnerability index value offers insights into the potential intensity of ground shaking resulting from earthquakes in a specific area. Local effects leading to damage during an earthquake are typically associated with a low dominant frequency (f_o) (longer period) and a high amplification factor (12–14). The seismic vulnerability index (K_g) demonstrates the correlation between the amplification factor and the dominant frequency of the soil (f_o).

3.5 Shear Wave Velocity (v_s)

Shear wave velocity (v_s) is a crucial soil parameter with various applications, including stratigraphic layer mapping, pre-construction site characterization studies, dynamic properties estimation, liquefaction potential assessment, and detection of underground features like cavities, tunnels, and sinkholes [20]. Shear wave velocity is primarily influenced by soil density, void ratio, and effective stress, while factors such as soil type, age, depositional environment, cementation, and stress history also play a role in determining v_s [21]. N-SPT data can be utilized to obtain v_s values, and several empirical equations exist for estimating v_s based on N-SPT data. One such approach is the empirical method proposed by Imai and Tonouchi (1982). The Imai and Tonouchi correlation was based on about 1650 experimental points in Japan, covering various types of soils, such as clay, silt, sand, and gravel. The Imai and Tonouchi correlation may be used for different site conditions when there is no site-specific correlation available or when the soil type is unknown. The calculation of v_s can be performed using the following equation [22]:

$$v_s = 96.9 \times N^{0.314} \tag{6}$$

Where v_s is the shear wave velocity (m/s) and N is the number of blows of N-SPT.

3.6 Geological Condition

According to Rahardjo et al. (1995), the oldest rock formations in the Opak River area include breccia-tuff, pumice breccia, dacite tuff, andesitic tuff, and tuffaceous claystone from the Semilir Formation (Tmse). Overlying the Semilir Formation is the Lower Miocene Nglanggran Formation (Tmn), which is composed of volcanic breccias, flow breccias, agglomerates, lavas, and tuffs. The Nglanggran Formation is further overlain by the Middle Miocene Sambipitu Formation (Tms), which consists of tuff, shale, siltstone, sandstone, and conglomerate. The Sambipitu Formation is followed by the Wonosari Formation (Tmwl), which is composed of marl and layered limestone and represents the Upper Miocene-Pliocene period, including reef limestone, calcarenite, and tufanic calcarenite. Additionally, the Sentolo Formation, located in the western part of the study area, is characterized by limestone and marl sandstone deposition (Fig.2)

The majority of the Yogyakarta-Bantul region is covered by Quaternary rock formations originating from the young Mount Merapi, which consist of tuff, volcanic ash, breccia, agglomerate, and lava flows. The youngest formations in the area are the alluvium formations (Qa), which consist of gravel, sand, silt, and clay found along major rivers, as well as sand from sand dunes and coastal areas [23].

4. RESULTS AND DISCUSSION

Nakamura's approach (1989) is based on the presence of a soft, weathered layer overlaying a hard bedrock layer. According to this approach, the H/V spectral ratio typically exhibits a peak that corresponds to the site's fundamental frequency (f_o) and peak amplitude (A_o) [24]. The level of ground amplification at a site is influenced by the impedance contrast between the loose, weathered layer and the rigid bedrock. Areas with high values of impedance contrast indicate higher amplification levels [25-27].

4.1 Characteristics of the Amplification Factor (A_o) in the Opak River

The amplification factor in the Opak River area ranges from 0.30 to 8.72, indicating the presence of deamplification, no change, and amplification of seismic wave amplitudes (Fig.5). Deamplification typically occurs in areas with compact and

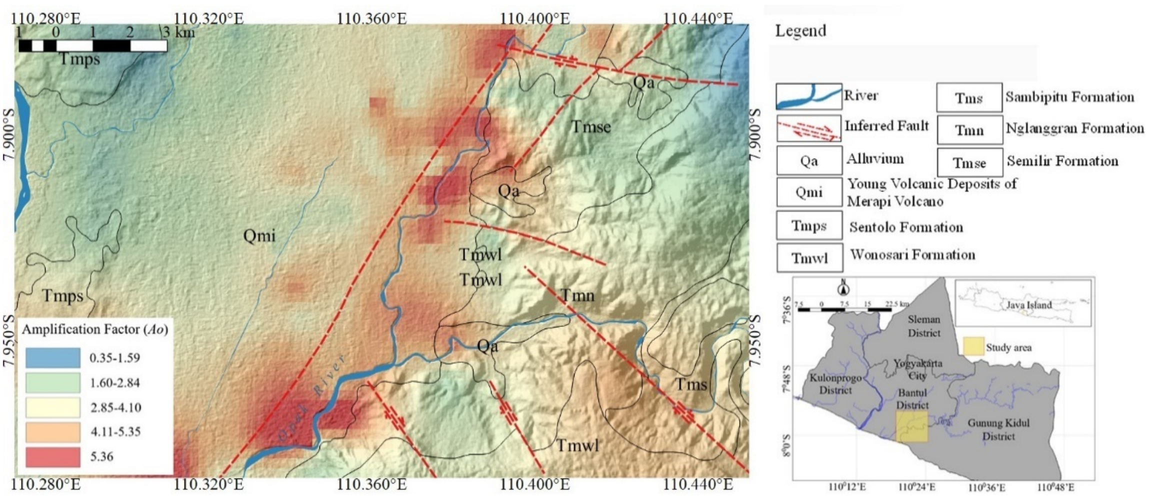

Fig.5 Microzonation of the Amplification Factor in the Opak River Area, the red and orange colors indicate an amplification factor > 4.1 along the Opak River channel.

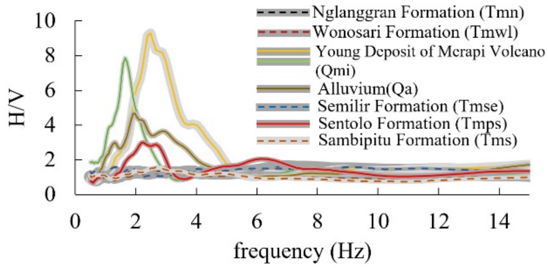

Fig.6 The H/V curve for each geological formation in the Opak River area; the clear peak of the curve is visible in the Qmi, Qa, and Tmps Formations.

consolidated materials [28]. Specifically, deamplification is observed in the Nglanggran Formation (Tmn) on the east side of the river and the Sentolo Formation (Tmps) on the west side. Formations such as Nglanggran (Tmn), Semilir (Tmse), Wonosari (Tmwl), Young Merapi Volcanic Deposits (Qmi), and Sentolo (Tmps) show no change in seismic wave amplitude.

The Young Merapi Volcanic Sediment Formation (Qmi) exhibits an amplification factor of 1 and is located further away from the Opak River channel, typically more than 2.5 km. The area surrounding the Opak River channel predominantly experiences amplification, with A_o values greater than one. This area is situated on the floodplain and alluvium of the Opak River, which contributes to a strong site-effect response [11-13]. The thickness of the alluvium layer in the Opak River area influences the amplification characteristics [29]. Amplification (A_o) in this area ranges from 1.1 to 8.72 and is associated with Qmi and Qa.

Comparing the HVSR curves in each formation reveals that the age of the formation determines the amplification factor value (Fig.6). HVSR curves with single or multiple peaks indicate the presence of one or more impedance contrasts beneath the observation sites. Resonance frequencies with lower H/V amplitudes indicate minor impedance contrasts, while sites with no discernible HVSR peak suggest very weak impedance contrasts beneath the site [30,31]. Formations of younger age (Quaternary age) exhibit higher amplification factor values compared to formations of later age (Tertiary age) [7]. This is reflected in the shape of the HVSR curve, with clear peak criteria observed in Quaternary age formations (Qmi and Qa) and tertiary Pliocene formations (Tmps). The mean A_o values for Quaternary Age formations (Qmi and Qa) are 4.5 and 4.4, respectively, while they are 2.2 and 2.3 for Pleistocene Tertiary Age formations (Tmps and Tmwl) (Table 1). The mean A_o values for Miocene Tertiary Age formations (Tms, Tmn, and Tmse) are 2.5, 2.3, and 1.9, respectively (Table 1).

Table 1 The Value of A_o in The Opak River

Formation	A_o		
	Max	Min	Average
Qmi	8.72	3.00	4.50
Qa	5.70	2.50	4.40
Tmps	3.70	1.00	2.28
Tmwl	3.71	1.17	2.17
Tms	3.58	1.56	2.49
Tmn	4.83	0.40	2.35
Tmse	4.55	0.30	1.86

The trend of A_o values in each formation indicates that younger formations with unconsolidated lithology tend to have higher A_o values compared to older formations, which are predominantly characterized by consolidated and compact lithology (Fig.7).

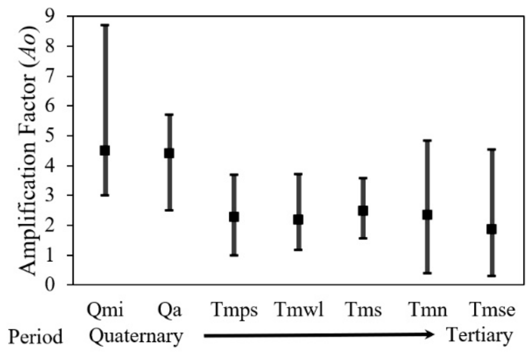

Fig.7 The value of maximum, minimum, and average A_o by formation.

4.2 Characteristics of Dominant Frequency (f_o) and Weathered Layer Thickness (h) in the Opak River

The dominant frequency is used to describe the physical characteristics of the soil either at the surface or below the soil surface. A lower predominant frequency value indicates the presence of a thick or weathered layer in the area, while a higher value suggests the presence of harder rocks or thinner weathered layers [32]. In the Opak River area (Fig.8), the dominant frequency ranges from 0.52 to 20.17 Hz. Areas with f_o > 6.7 Hz are associated with thin weathered layers and are predominantly located in tertiary age formations (Tmps, Tmwl, Tms, Tmn, and Tmse) [7, 35]. The characters fo and h in each formation can be seen in the distribution of the maximum, minimum, and average values of the two parameters (Tables 2-3). This value is obtained based on descriptive statistical analysis at the measuring points found in each formation.

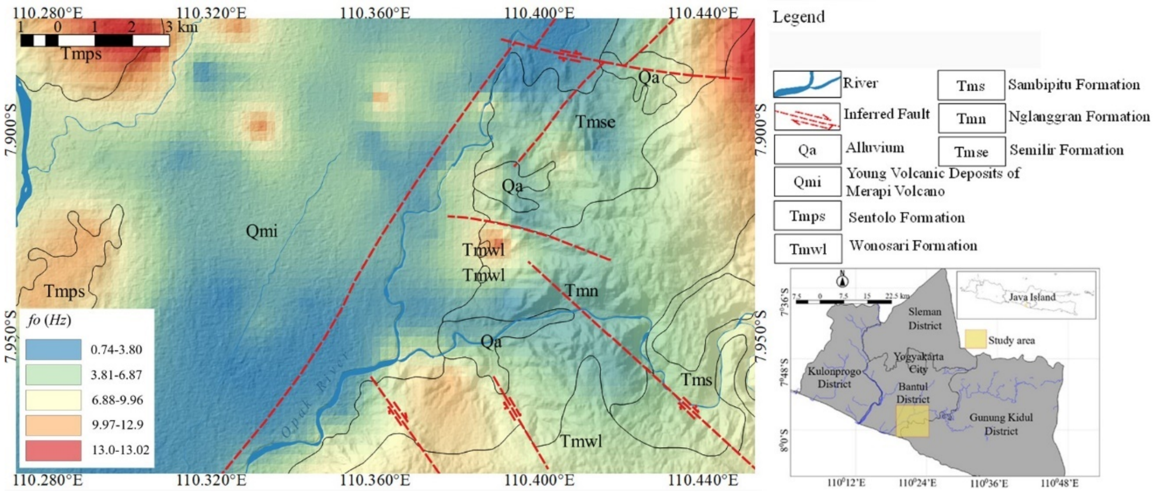

Fig.8 Microzonation of f_o in the Opak River area: yellow to red indicates areas with f_o > 6.7 Hz (a thin weathered layer with dominant hard rock). The blue color represents an area with f_o 2.5 Hz (thick weathered layer > 30 meters) that is dominant in the Opak River channel area.

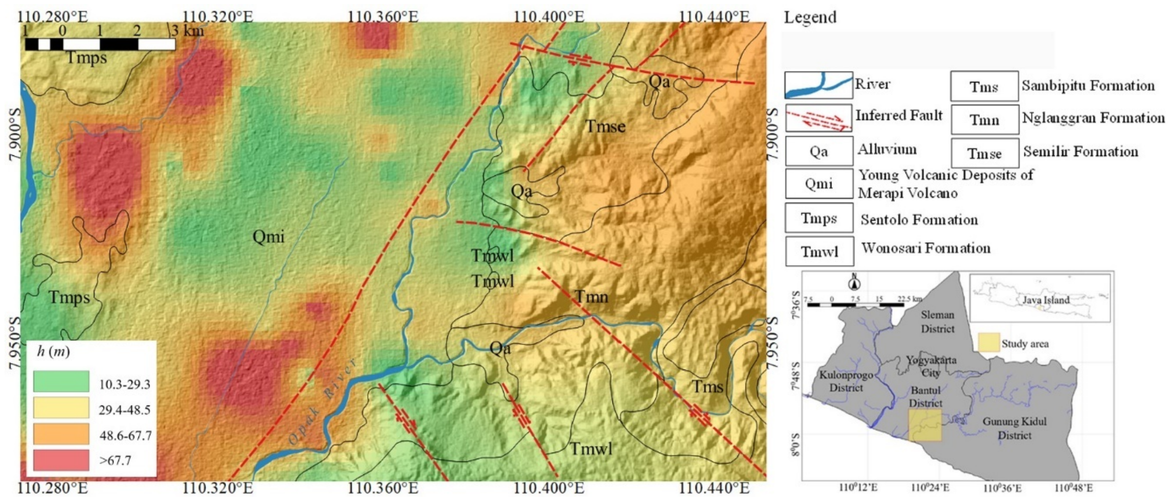

Fig.9 Microzonation of weathered layer thickness in The Opak River area, red color indicates weathered layer thickness > 60 m and is dominant in the Qmi Formation. Green color represents a layer thickness >30 m.

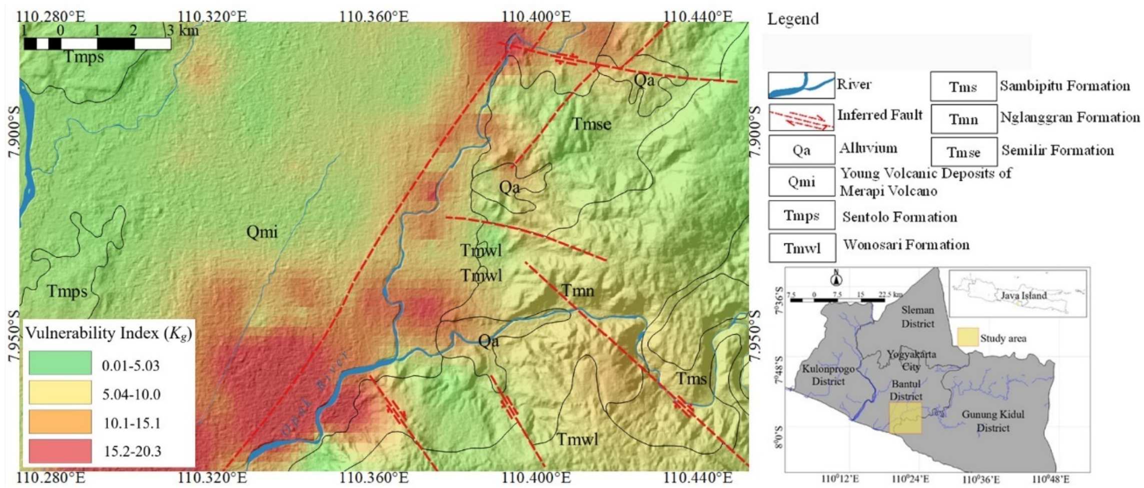

Fig.10 Microzonation of the Seismic Vulnerbalitiy Index (K_g) in the Opak River area: a red color with K_g > 20 indicates an area that has the potential to be affected by seismic waves if an earthquake occurs. The area is concentrated along the Opak River and is in the Qmi Formation.

On the other hand, areas with f_o < 2.5 Hz are related to thick weathered layers characterized by unconsolidated sedimentary material, which primarily corresponds to Quaternary formations (Qmi and Qa) [7]. The average f_o values for Quaternary formations with a frequency ≤ 6 Hz are 2.52 Hz for the Qmi Formation and 5.63 Hz for the Qa Formation. For Tertiary formations with a frequency ≥ 6 Hz, the values are 8.26 Hz for Tmps, 8.30 Hz for Tmwl, 8.39 Hz for Tms, 8.93 Hz for Tmn, and 5.69 Hz for Tmse (Table 2).

The microtremor approach provides insights into the thickness of the weathered layer, which ranges from 5.47 to 136.46 m (Fig.9). The thickest weathered layer is found in the Qmi Formation, measuring 136.46 m, while the Tmps Formation has the thinnest layer at 5.47 m. The trend of weathered layer thickness based on formation age shows an inverse relationship with the predominant frequency. Older formations (Tertiary) tend to have thinner, weathered layers (h) and higher predominant frequencies (f_o). The average h values for Quaternary formations are >31 m, specifically 37.94 m for the Qmi Formation and 33.02 m for the Qa Formation. For tertiary formations with a thickness >31 m, the values are 11.57 m for Tmps, 20.41 m for Tmwl, 30.85 m for Tms, 17.59 m for Tmn, and 27.07 m for Tmse (Table 3).

Table 2 The Value of f_o in The Opak River

Formation	f_o (Hz)		
	Max	Min	Average
Qmi	10.28	0.52	2.52
Qa	18.46	1.18	5.63
Tmps	13.00	2.70	8.26
Tmwl	19.87	0.66	8.30
Tms	15.57	1.06	8.39
Tmn	20.17	1.12	8.93
Tmse	15.88	0.80	5.69

Table 3. The Value of h in The Opak River

Formation	h (m)		
	Max	Min	Average
Qmi	136.46	6.92	37.94
Qa	59.83	8.83	33.02
Tmps	26.15	5.47	11.57
Tmwl	41.16	12.33	20.41
Tms	35.71	26.73	30.85
Tmn	42.32	5.51	17.60
Tmse	41.58	8.46	27.07

4.3 Seismic Vulnerability Index (K_g) in The Opak River

In various studies, K_g represents the impact of seismic wave propagation in terms of damage to building structures, liquefaction, and local site effects [33–37]. The K_g values in the Opak River area range from 0.01 to 20.25 (Fig.10). The distribution of K_g values exceeding 20, which indicates the potential for causing damage [13], is predominantly observed in the Qmi Formation, located around the Opak River channel (Fig.12a). This distribution pattern of K_g values >20 follows the flow of the Opak River from the southwest to the northeast and is associated with the Opak Fault. The trend of K_g values based on formation age reveals that formations of Quaternary age exhibit higher maximum, minimum, and average values compared to formations of Tertiary age (Fig.11).

The Quaternary-aged Qmi and Qa Formations have an average K_g value ranging from 6.85 to 8.73, while the Tertiary-aged Tmps, Tmwl, Tms, Tmn, and Tmse Formations (Fig.12b) have an average K_g value ranging from 1.23 to 1.77 (Table 3).

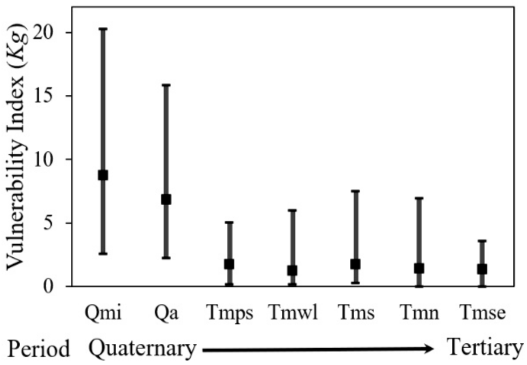

Fig.11 The values of average, maximum, and minimum K_g based on formation age.

Table 3. The Value of K_g in The Opak River

Formation	K_g		
	Max	Min	Average
Qmi	20.25	2.61	8.73
Qa	15.86	2.23	6.85
Tmps	5.07	0.20	1.77
Tmwl	6.01	0.19	1.24
Tms	7.50	0.27	1.77
Tmn	6.93	0.01	1.40
Tmse	3.59	0.01	1.35

The spatial distribution of high K_g zones (Fig.10) and the observed damage after the Mw 6.3 Yogyakarta Earthquake (Fig.1) exhibit a consistent pattern. The distribution of damage to buildings in the category of extensive and moderate damage was concentrated in areas along the Opak River channel with the Qmi and Qa formations. The area has a value of kg >20, which indicates potential damage due to an earthquake. However, it is important to note that the damage to building structures is influenced by multiple factors [3].

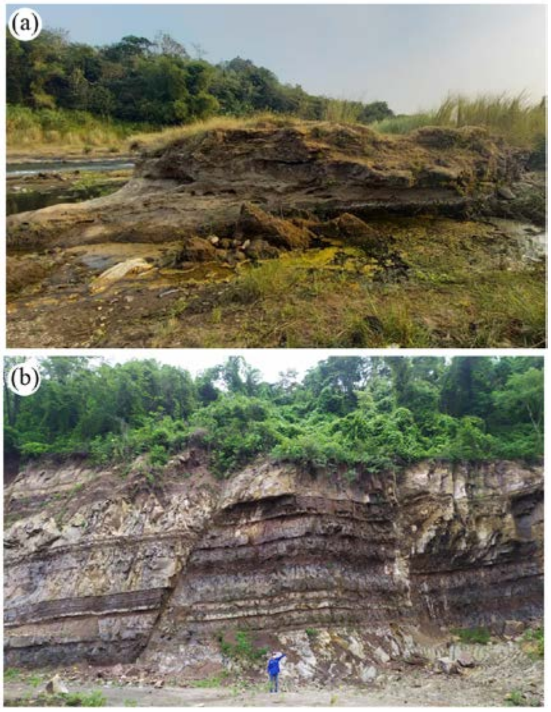

Fig.12 (a) The Opak River basin area in the Qmi Formation, which is in the K_g zone >20, is made up of unconsolidated material with sand. (b) The Segoroyoso area in the Tmse Formation, which is in the K_g < 5 zone, is composed of interbedded tuff breccia, pumice breccia, dacite tuff, andesite tuffs, and tuffaceous claystone.

4.4 Characteristics of Lithology and The Average Shear Wave Velocity ($\overline{v_s}$) in the High Vulnerability Index (K_g) Zone

The zone with high K_g values is located in the Qmi Formation along the Opak River channel. The N-SPT data from Segoroyso, Karangsemut, and Tempuran Opak can be used to calculate lithology and $\overline{v_s}$ values in this high K_g zone. Common lithologies in the high K_g area include sand, clay, silt, and breccia. In the Segoroyoso area, sand dominates with interspersed clay and breccia layers (Fig.13a). The breccia layer was found at a depth of 10.25m with a thickness of 8m. According to the microtremor approach, the weathered layer thickness in the Segoroyoso area is 15.64m, with an A_o value of 1.51. The weathered layer consists of sand (depth 0–6.25m), clay (depth 6.26–8.25m), sand (depth 8.26–10.25m), and breccia (depth 10.26–15.64m). The value of $\overline{v_s}$ based on the N-SPT approach in the Segoroyo area is 287 m/s. In the Karangsemut area, the lithology includes sand, silt, and clay. The first layer has a sand thickness of 10.22m, while the fourth layer has a thickness of 6.0m (Fig.13b). According to the microtremor approach, the weathered layer thickness is 24.66m, representing a layer of sand from a depth of 14.26m that can continue to a depth of 24.66m. The weathered layer is thick and composed of sand (depth 0-10.25m), silt (depth 10.26–12.25m), clay (depth 12.26–14.25m), and sand (depth 14.26–24.66m). The Karangsemut area has a thick weathered layer with an Ao value of 5.04. The value of $\overline{v_s}$ based on the N-SPT approach in the Karangsemut area is 279 m/s. In the Opak Tempuran area (Fig.13c), the N-SPT profile indicates the presence of sand and breccia. The sand layers range in depth from 0 to 12.25m, while the breccia layers range in depth from 12.26 to 26.25m. Using the microtremor method, the weathered layer thickness in the area is determined to be 9.59m, primarily related to the presence of a sand layer, with an A_o value of 3.92. The value of $\overline{v_s}$ based on the N-SPT approach in the Opak Tempuran area is 293.67 m/s.

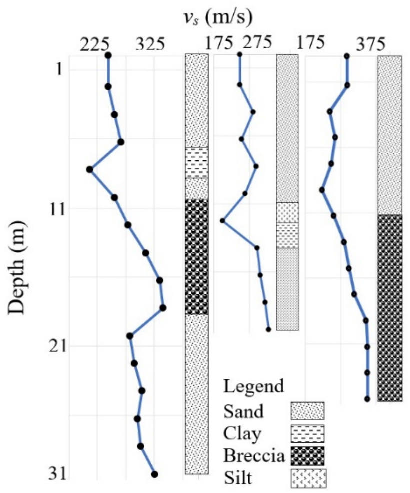

Fig.13 Lithology and v_s values in the N-SPT data are determined using the Imau and Tonouchi equations: (a) the Segoroyoso area, (b) the Karangsemut area and (c) the Tempuran Opak area.

N-SPT data can be used to identify lithology in Pranti, Bambanglipuro, Wijirejo, and Watu locations with moderate K_g criteria. The lithology of the Pranti region (Fig. 14a) includes sand, clay, and breccia. Sand layers dominate to a depth of 28.25 meters, with clay inserts at 8.25 and 28.25 meters. The seismic parameters at this site are h 16.13 m, K_g 5.73, and A_o 4.07, indicating that despite the fact that the lithology is dominated by sand, this area is rather secure from earthquakes.

Based on the N-SPT method, the value of $\overline{v_s}$ in the Pranti area is 263 m/s. The lithology of the Bambanglipuro area (Fig.14b) is relatively more complex, with layers of sand, sandstone, clay, and breccia. The average sand layer thickness at this site is 8 m, followed by 6 m of sandstone, 2 m of clay, and 4 m of breccia. Based on microtremor measurements, the seismic parameters are h 38.67 m, K_g 6.18, and A_o 3.04. Based on the N-SPT method, the value of $\overline{v_s}$ in the Bambanglipuro area is 282 m/s. The lithology of the Wijirejo area (Fig. 14c) contains sand, sandstone, and clay. The sand and sandstone layers dominate with thicknesses of 16 m and 12 m, respectively, and the seismic characteristics at this position are h 53.16 m, K_g 0.85, and A_o 1.46. Based on the N-SPT method, the value of $\overline{v_s}$ in the Wijirejo area is 285 m/s. The N-SPT profile in the Watu area (Fig.14d) shows the presence of sand, silt, clay, breccia, and sandstone. With a thickness of 10 m, the sand and sandstone layers dominate, while the seismic parameters at this site are h 30.86 m, K_g 10.66, and A_o 3.79. Based on the N-SPT method, the value of $\overline{v_s}$ in the Watu area is 272 m/s.

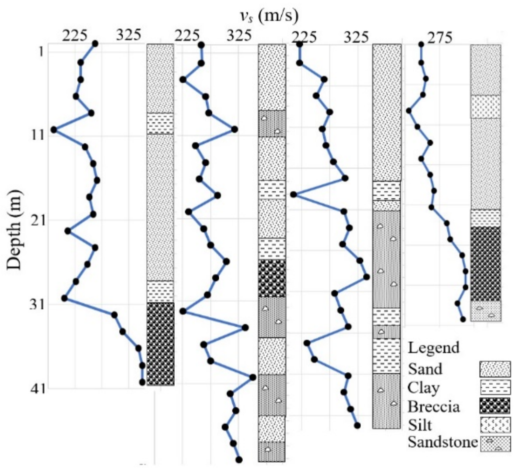

(a) (b) (c) (d)

Fig.14 Lithology and v_s values in the N-SPT data are determined using the Imau and Tonouchi equations: (a) the Prati area, (b) the Bambanglipuro area, (c) the Wijirejo and (c) the Watu area.

5. CONCLUSION

Depending on their formation chronology, geological formations respond differently to seismic wave propagation. The Opak River area can be categorized into two groups based on their ages: Quaternary formations (Qmi and Qa) and Tertiary formations (Tmps, Tmwl, Tms, Tmn, and Tmse). The average A_o values in the Qmi and Qa Formations exceed 4.4, while the Tmn, Tmse, Tmwl, and Tms Formations have average A_o values below 3. Tertiary formations (Tmps, Tmwl, Tms, Tmn, and Tmse) exhibit an average f_o greater than 5 Hz, with the Tmn Formation having the highest f_o and the Qmi Formation having the lowest f_o. Tertiary-age formations (Tmps, Tmwl, Tms, Tmn, and Tmse Formations) have an average h value below 30 m. The Quaternary formations (Qmi and Qa Formations) exhibit the highest average K_g values. In the Quaternary formations (Qmi and Qa Formations), areas with K_g values exceeding 20 are predominant, accompanied by $\overline{v_s}$ value ranging from 279 to 293.6 m/s. The lithology in the high K_g region (>20) consists of sand, silt, clay, and breccia elements, with the sand layer thickness being dominant.

Based on the seismic parameters, there is a contrast between Quarternary and Tertiary formations. The potential for seismic vulnerability increases in proportion to the age of the younger formations. This is in accordance with data on the distribution of damage to buildings after Mw 6.3 Yogyakarta earthquake, which was concentrated in the Qa and Qmi Formations. This condition occurs because the Quaternary Formation (Qa and Qmi) is predominantly composed of unconsolidated sediment materials such as sand, silt, clay, and breccia. The N-SPT data shows that the dominant sand layer is thicker than the other materials in the Quaternary formation. According to the findings of this study, geological formations with a younger age exhibit a higher potential for seismic hazards and Quaternary formations need more attention in seismic hazard mitigation programs.

6. ACKNOWLEDGMENTS

The author gratefully acknowledges to BMKG for granting permission and providing support to pursue the doctoral program. Additionally, the author expresses gratitude to the Education and Training Center of BMKG for their scholarship support. Special thanks are extended to the Sleman Geophysics Station of BMKG for their valuable assistance during the site survey.

7. REFERENCES

[1] United States Geological Survey (USGS), M6.3 Java Earthquake of May 2006, National Earthquake Information, 2006, pp.1-140.

[2] Fathani T. F., Adi A. D., Pramumijoyo S., and Karnawati D., The determination of peak ground acceleration at Bantul Regency, Yogyakarta Province, Indonesia, The Yogyakarta Earthquake of May 27, 2006, Star Publishing, California, 2008, pp. 12.1-12.15.

[3] Koseki J., Yoshimine M., Hara T., Kiyota T., Wicaksono R. I., Goto S., Agustian Y., Damage Survey Report on May 27, 2006, Mid Java Earthquake Indonesia, Soils and

Foundations, Vol. 47, Issue 5, 2007, pp. 973-989.

[4] BAPPENAS, Preliminary Assessment of Damage and Loss of Natural Disasters in Yogyakarta and Central Java, 15th Meeting of the Consultative Group for Indonesia, 2006, pp. 1-137.

[5] Seshunarayana T., Trupti S., Goverdhan K., Srinivas S. S. S., Kishore P. P., Horizontal to vertical spectral ratio in different geological formations, *Arab J Geosci* 6, 2013, pp. 4215–4223. https://doi.org/10.1007/s12517-012-0696-1.

[6] UN Cluster Atlas, Java Earthquake Response — One Year Review, United Nations Coordination Centre for Yogyakarta and Central Java and the Office of the Resident/ Humanitarian Coordination in Indonesia. Compiled from the One Year Commemoration Conference, 25 – 27 May 2007, Yogyakarta, 2007, pp. 1-125.

[7] UNOSAT, Preliminary Damage Assessment–Java Earthquake, 2006, http://unosat.web.cercn.ch/unosat/.

[8] Rahardjo, Sukandarrumidi W., and Rosidi H., Geologic map of the Yogyakarta quadrangle, Java, scale 1:100,000, Geol. Surv. of Indonesia, Minist. of Mines, Jakarta, 1997, pp. 1-8.

[9] Borcherdt R. D., Glassmoyer G., Der Kiureghian A., and Cranswick E., Results and Data from Seismologic and Geologic Studies Following Earthquakes of December 7, 1988, near Spitak, Armenia S.S.R. USGS Numbered Series, Open File Report, 1989, pp. 89-163A.

[10] Ansal A., Biro Y., Erken A., and Guleru U., Seismic Microzonation: A Case Study. In A. Ansal (Ed.), Recent Advances in Earthquake Engineering and Microzonation, Kluwer Academic Publishers, Vol. 1, 2004, pp. 253-256.

[11] Nakamura Y., Real-Time Information Systems for Hazards Mitigation. Proceedings of the Xth World Conference on Earthquake Engineering, Acapulco, 23-26 June 1996, 2134.

[12] Nakamura Y., Seismic Vulnerability Indices for Ground and Structures Using Microtremor. World Congress on Railway Research, Florence, Italy, November 1997, pp. 1-7.

[13] Nakamura Y., Clear Identification of the Fundamental Idea of Nakamura's Technique, and Its Applications. 12th World Conference on Earthquake Engineering, New Zealand (CD-ROM) Paper No. 2656, 2000.

[14] Bard P.Y., Bourjot L., and Sesame Team., Guidelines for The Implementation of The H/V Spectral Ratio Technique on Ambient Vibrations Measurements, Processing and Interpretation, European Commission - Research General Directorate Project No. EVG1-CT-2000-00026 SESAME, 2004, pp. 1-63.

[15] Noguchi T., Nishimura I., Ono Y., and Kohno M., Estimation of Subsurface Structure Based on Microtremor and Seismic Observations in Area Damaged by 2018 Hokkaido Eastern Iburi Earthquake, Hokkaido, Japan, International Journal of GEOMATE, Vol. 20, Issue 81, 2021, pp. 8–15. DOI: https://doi.org/10.21660/2021.

[16] Nakamura Y., A method for dynamic characteristics estimation of subsurface using microtremor on the ground surface. Quarterly Report of Railway Technical Research 30, 1989, pp. 25-33.

[17] Takai and Tanaka, On microtremors VIII, Tokyo: Bull. Earthquake Res, Inst 39, 1961, pp. 97-114.

[18] Kawase H., Aki K., A study on the response of a soft basin for incident S, P, and Rayleigh waves with special reference to the long duration observed in Mexico City, Bulletin of the Seismological Society of America 79. Vol. 5, 1989, pp. 1361-1382.

[19] Ibs-von S. M., and Jtirgen W., Microtremor Measurements Used to Map Thickness of Soft Sediments, Bulletin of the Seismological Society of America, Vol. 89, No. 1, 1999, pp. 250-259.

[20] Seed H. B., Idriss I. M., and Arango I., Evaluation of liquefaction potential using field performance data, Journal of Geotechnical Engineering, 109, 1983, pp. 458–482.

[21] Hardin B. O., and Drnevich V. P., Shear modulus and damping in soils: design equations and curves, J. Soil Mech. and Foundations Div., SM 7, 1972, pp. 667–692.

[22] Imai T., and Tonouchi K., Correlation of N-value with S-wave velocity and shear modulus, Proc. 2nd European Symp of Penetration Testing (Amsterdam), 1982, pp. 57–72.

[23] Santoso dan Siregar D. A., Morfologi dan Umur Perpindahan Alur Sungai Opak di Daerah Berbah Sleman, Jurnal Geologi dan Sumberdaya Mineral. Vol. 19, No. 2, 2009, pp. 117-126.

[24] Mohamed A., El khateeb S. O., Dosoky W., and Abbas M. A., Site Effect Estimation Using Microtremor Measurements at New Luxor City Proposed Site, South Egypt. Journal of Geoscience and Environment Protection, Vol. 9, 2021, pp. 131-149.

[25] SESAME, Guidelines for the Implementation of the H/V Spectral Ratio Technique on Ambient Vibrations: Measurements, Processing and Interpretation, SESAME European Research Project WP12, 2004, pp. 1-62.

[26] Partono W., Irsyam M., Nazir R., Kistiani F, and Sari U. C., Development Of Site Factor For Surface Spectral Acceleration Calculation At The Alluvial Soils, International Journal of GEOMATE, Vol. 23, Issue 98, 2022, pp. 24–30.

[27] Molnar S., Cassidy J. F., Castellaro S., Cornou C., Crow H., Hunter J. A., Matsushima S., Sanchez-Sesma F. J., and Yong A., Application of Microtremor Horizontal-to-Vertical Spectral Ratio (MHVSR) Analysis for Site Characterization: State of the Art. Surveys in Geophysics, No. 39, 2018, pp. 613-631.

[28] Ohta H., Hagino Y., Udaka T., Demura Y., Atushi I., Seismic deamplifying effect of soft clay layers, 14th International Conference on Soil Mechanics and Foundation Engineering (Hamburg), 1997, pp. 859-862.

[29] Teves-Costa P., Matias L., Bard P. Y., Seismic Behaviour estimation of thin alluvium layers using microtremors recordings. Soil Dyn. Earthq. Eng, 1996, pp. 201-209.

[30] Kang S. Y., Kim, K-H., Kim D., Jeon B-U., and Lee J-W., Effects of meteorological variations and sensor burial depths on HVSR analysis, J. Korean Earth Sci. Soc. 41, 2020, pp. 658–669.

[31] Singh A. P., Sairam B., Pancholi V., Chopra S., and Kumar M. R., Delineation of thickness of intrabasaltic rocks beneath the Deccan Volcanic province of Western India through microtremor analysis. Soil Dyn. Earthq. Eng, Vol.138, 2020, 106348.

[32] Supriyadi, Khumaedi, Sugiyanto, Akhmad F. R., Wahyu M. H., Study of The Subsurface Structure Based on Microseismic Data in The Heritage Area of Kota Lama Semarang, Indonesia, International Journal of GEOMATE, Vol. 23, Issue 97, 2022, pp. 211-219.

[33] Nishimura I., Noguchi T., Kagawa T., Estimation of Subsurface Structures and Ground Motion Characteristics in The Areas Damaged in the 2016 Central Tottori Prefecture Earthquake In Japan, International Journal of GEOMATE, Vol. 20, Issue 82, 2021, pp. 15–21. DOI: https://doi.org/10.21660/2021.82.

[34] Hardesty K., Wolf L. W., and Bodin P., Noise to signal: A microtremor study at liquefaction sites in the new Madrid seismic zone, Geophysics 75, 2010, pp. B83–B90.

[35] Singh A. P., Shukla A., Kumar M. R., and Thakkar M. G., Characterizing surface geology, liquefaction potential, and maximum intensity in the Kachchh seismic zone, Western India, through microtremor analysis, Bull. Seismol. Soc. Am, Vol. 107, 2017, pp. 1277–1292.

[36] Farid M., and Mase L. Z., Implementation of seismic hazard mitigation on the basis of ground shear strain indicator for spatial plan of Bengkulu city, Indonesia, International Journal of GEOMATE, Vol. 18, Issue 69, 2020, pp. 199–207.

[37] Kang S. Y., Kim K-H., Choi, M., and Park S-C., Ground vulnerability derived from the horizontal-to-vertical spectral ratio: Comparison with the damage distribution caused by the 2017 ML 5.4 Pohang earthquake, Korea. Near Surf. Geophys, Vol. 19, 2021, pp. 155–167.

.